Romanian Reports in Physics **XX**, XYZ (2017)

PHOTON LUMINESCENCE STUDIES OF TETRAHYDROFURAN FOLLOWING TRIHYDROGEN CATIONS IMPACT IN THE 20-1000 EV ENERGY RANGE

TOMASZ J. WASOWICZ

Division of Complex Systems Spectroscopy, Institute of Physics and Applied Computer Science,
Faculty of Applied Physics and Mathematics, Gdansk University of Technology,
ul. G. Narutowicza 11/12, 80-233 Gdańsk, Poland
E-mail*: tomasz.wasowicz1@pg.edu.pl*

Received

Abstract. Photon emission arising during tetrahydrofuran (C_4H_8O, THF) fragmentation initiated by H_3^+ ion impact has been studied experimentally. Luminescence fragmentation spectra and the relative emission cross-sections of the excited fragments have been measured using collision-induced emission spectroscopy in the 20-1000 eV energy range. The main features in the spectra are the H Balmer series lines, whose intensities decrease with increasing principal quantum number *n* more quickly than predicted by quantum theory. Optical spectra also display weak emission of vibrationally and rotationally excited diatomic CH fragments. The possible mechanisms leading to the observed products are discussed.

Key words: tetrahydrofuran, collisions, charge-transfer, dissociation, luminescence.

1. INTRODUCTION

Studies on ion-molecule interactions decipher numerous processes in astrochemistry, medicine, and engineering. In interstellar media, they are the ground reactions underlying cosmochemistry. The astrophysicists believe that ionic bombardment could have been an essential factor in the appearance and fostering of nascent life on Earth as cosmic rays irradiated increasingly complex compounds, converting them into the prebiotic biomolecules [1], [2]. Ion-molecule reactions are also highly relevant in hadron therapies in radiation damage to the cancerous cells [3],[4]. The interaction of charged particles with malignant tumors produces physical and chemical modifications by bond cleavages in the structural subunits of cells. These lesions are caused by the primary ionizing beams and the secondary particles (electrons, ions, radicals, excited atoms, and molecules) formed within the track [4]. Ionic interactions with the matter have other exciting applications. Investigations of the fundamental aspects of the etching and deposition processes induced by focused ion beams (FIB) have immense potential for developing ion beam processing and fabrication techniques [5]. Moreover, fragmentation and 3D

mapping down to a feature size of 20–30 nm of the living cells adsorbed on the surfaces using FIB etching allow tracing the connectivity of Eukaryotic cell traffic routes [6].

In ion-molecule interactions, the heterocyclic compounds are vital since many of these molecules are critical for life processes and build mixtures used in industry and technology. In this context, tetrahydrofuran molecule is used as the most straightforward analog to deoxyribose (dR) sugar [7], [8], and as a precursor to polymers [9]. Accordingly, ionization and fragmentation of this compound have been extensively studied by both experimental and theoretical methods [10]-[20].

Photon luminescence investigations of THF following ion impact are scarce. The only studies are that of Wasowicz & Pranszke [19], [20], who used collision-induced emission spectroscopy to explore collisions of tetrahydrofuran molecules with positively charged atomic ions such as protons (H^+), carbon (C^+), and oxygen (O^+) cations. They obtained emission spectra in the wavelength of 200-520 nm and the 5-1000 eV energy range and showed that the cation-induced dissociation mechanisms depend on the projectile mass and electron density. However, to the best of our knowledge, no experimental or theoretical data were reported previously on molecular ions impinged upon THF molecules. Therefore, the present work focuses on unraveling the processes occurring in the gas-phase tetrahydrofuran molecules under trihydrogen cations (H_3^+) impact using the optical spectroscopic methods in the energy range from 20 to 1000 eV, which corresponds to velocities of 35−254 km/s. A positively charged H_3^+ ions were selected as projectiles for the present study because of two reasons. The H_3^+ consisting of three hydrogen atoms sharing two valence electrons is the simplest triatomic molecular ion, and it is one of the most abundant molecular ions formed in the interstellar clouds and the planet ionospheres [21]-[22]. In hadron therapies, on the other hand, tumors are mostly exposed to the proton, and C^+ projectiles [23]-[25], but current studies are performed to applicate other ionic beams [25]-[27]. Thus, the H_3^+ can be potentially applied to probe the molecule-molecule collisions in those environments.

2. EXPERIMENTAL METHOD

The experimental setup was described earlier [28], but pertinent comments are added here. The most extensive description of this apparatus with its pluses and minuses was presented in the papers [20], [29]. Moreover, the sketch of the apparatus and measuring methods were described in [19].

The setup consisted of four chambers containing: the ionic source, the magnetic mass selector, the collision cell, and the optical spectrometer. Trihydrogen cations were created from the molecular hydrogen gas under pressure of 100 Pa utilizing an ionic source of the Colutron hot cathode discharge type.

Generated ions were extracted from the ion source using 1000 V voltage and directed to the second chamber with a 60° magnetic mass selector, which separated them according to the m/q ratio. The selected cations were then slow down to the required energy and transferred to the collision chamber. There they impinged upon the vapors of the THF molecules. Some fragments/products in excited states occurred as a result of such collisions. The lifetimes of these products are sufficiently short that these particles emit all the light in the collision region. The optical emissions were then recorded with a sensitive, multi-channel photon detector mounted in the optical spectrometer. The detection system was equipped with two gratings differing in the number of lines per mm. The first grating had 1200-l/mm and allowed measuring the high-resolution spectra $\Delta\lambda$ of 0.4 nm (FWHM) appropriate to identify the spectral components accurately. The second one had 300-l/mm and allowed recording the luminescence spectra with higher intensity but a lower optical resolution ($\Delta\lambda$ of 2.5 nm). The 300-l/mm grating was employed to record a specific spectral feature luminescence as a function of the energy/velocity of incident cations. Ion beam energies were set in the range of 20-1000 eV. These energies corresponded to velocities of about 35-254 km/s. Each spectrum in this regime was corrected for the wavelength dependence of the optical system sensitivity. The calculated intensities were then normalized to the cation beam current (nA), recording time (s), and pressure (mTorr). This "emission function" provided us with a relative emission cross-section (σ) or, in other words, the formation probability of the studied product. It is of note that the velocity dependence of emission functions enables direct comparison of cross-sections obtained in various collisional systems.

The anhydrous tetrahydrofuran sample was purchased from Sigma Aldrich. A declared purity was 99.9%. THF is liquid at room temperature (~20 °C), but due to high vapor pressure (143 mmHg) [30], it can be measured without heating the sample. THF was only degassed through several freeze-pump-thaw cycles at the beginning of the experiment. During the experiment, the pressure of the THF gas was kept constant at 15 mTorr, as determined with the Barocel capacitance manometer.

3. RESULTS AND DISCUSSION

3.1. LUMINESCENCE SPECTRA

In Fig. 1, the high-resolution luminescence fragmentation spectrum recorded for collisions between the H_3^++C_4H_8O at the energy of 1000 eV is presented. It displays intense atomic lines of the Balmer series, H_β to H_ζ, arising via excitation of hydrogen atoms to n = 4-8 states, respectively. These intensities decrease rapidly with increasing principal quantum number n. The excited CH

diatomic molecules are also identified by the emission of the molecular systems of ($A^2\Delta \rightarrow X^2\Pi_r$) and ($B^2\Sigma^- \rightarrow X^2\Pi_r$).

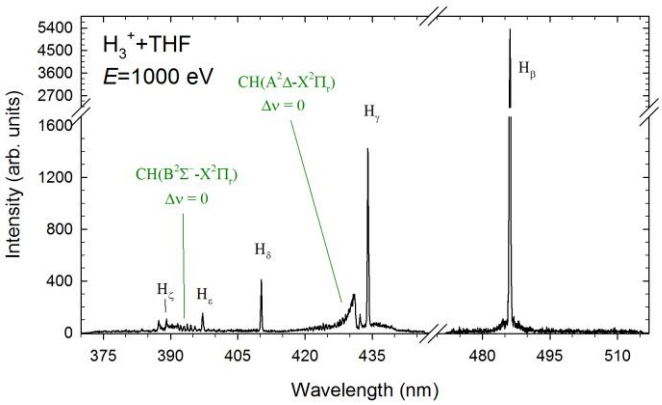

Fig. 1 – (Color online). Luminescence fragmentation spectrum measured with an optical resolution of $\Delta\lambda$=0.4 nm (FWHM) for H_3^+ + tetrahydrofuran collisions. The spectrum was not corrected for the wavelength dependence of the sensitivity of the detection system.

Present results can be directly compared with our earlier impact studies on tetrahydrofuran and its hydrogenated analogue – furan. For instance, we recorded very similar spectra in the H^++THF [19] and H^++Furan [20] collisions. However, emission spectra measured in the case of tetrahydrofuran molecules bombarded by heavier hadrons (C^+ and O^+) showed more intensive bands of CH radical and quite strong luminescence of the C atoms [19]. The fluorescence spectrum measured in the studies of photodissociation of THF [16] also revealed pronounced intensities of the diatomic CH fragments formed in the $A^2\Delta$ and $B^2\Sigma^-$ electronic states as well as weak fluorescence of the C_2 fragments in the $d^3\Pi_g$ excited state. Present spectrum may also be compared to the emission spectra obtained in the cation- [31]-[33], electron- [34], [35], and photon-induced [36]-[39] fragmentation of other five- and six-membered heterocyclic molecules. In contrast to the present measurement, all these investigations show major fragmentation of the target molecules into several excited atomic and molecular fragments. This comparison demonstrates that collisions with trihydrogen cations like collisions with protons do not efficiently dissociate the target molecules.

3.2. RELATIVE EMISSION CROSS-SECTIONS

Figures 2 and 3 show the H(*n*) and CH($A^2\Delta$; $B^2\Sigma^-$) relative emission cross-sections. The experimental uncertainties are the mean-standard deviations obtained from independent measurements performed at fixed projectile energies. Due to the ion beam energy spread and thermal motion of the target, the maximal uncertainty of collision energy was estimated to be 3.5% [40].

The H(*n*) curves obtained in collisions of H_3^+ with tetrahydrofuran (Fig. 2) show no production of the hydrogen atoms below 98 km/s (500 eV), but above 100 km/s, they increase rapidly with velocity up to 179 km/s (500 eV). They become almost constant between 180-234 km/s, and above 234 km/s (850 eV), they again increase. It is of note that the H(*n*) relative emission cross-sections obtained previously for protons [20] increase very similarly. Such resemblance may suggest that excited hydrogen atoms were produced in both collisional systems due to similar physical processes.

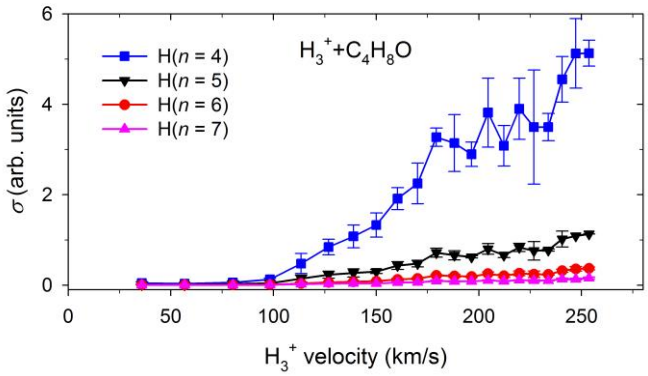

Fig. 2 – (Color online). The H(*n*) relative emission cross-sections obtained in collisions of H_3^+ with tetrahydrofuran molecules.

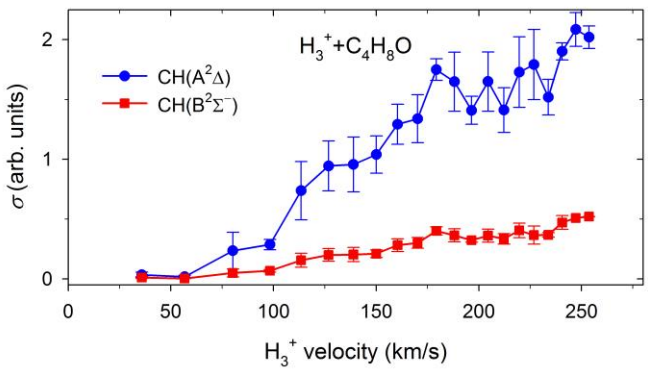

Fig. 3 – (Color online). The relative emission cross-sections of the CH($A^2\Delta$) and CH($B^2\Sigma$) fragments obtained in collisions of H_3^+ with tetrahydrofuran molecules.

The CH($A^2\Delta$) function obtained in the H_3^++THF collisions (Fig. 3) shows no production of CH fragments below 57 km/s (50 eV). Above 60 km/s, the CH($A^2\Delta$) yield increases gradually. The CH($B^2\Sigma^-$) function rises very similarly, but it has four times smaller values at maximum. In opposition, the CH($A^2\Delta$) emission cross-section measured previously in the H^++THF collisions differs from the present

curve. It rises slowly, almost linearly, with increasing velocity. Additionally, above 100 km/s, it is two times lower than the yield obtained in the H_3^++THF collisions. The comparison demonstrates that although trihydrogen cations do not significantly fragment the THF molecule, they still can decompose it more effectively than protons.

3.3. COLLISIONAL PROCESSES

Full details of the possible fragmentation pathways of tetrahydrofuran have been presented earlier elsewhere [16], [17], [19], and therefore in this paper, we limit the discussion only to the most pertinent facts.

Formation of the products observed can be initiated by four collisional mechanisms [19], [20], i.e., a single electron transfer, dissociative ionization, dissociative excitation, cation-molecule complex generation. The first process involves an electron capture from C_4H_8O to the H_3^+ projectile, which becomes neutral (i.e., H_3), followed by fragmentation of molecular parent cation $C_4H_8O^+$. The electron capture process occurs at rather long projectile−target distances corresponding to relatively high velocities of projectiles [41]-[47]. In the second mechanism, the target molecule is directly ionized and undergoes further fragmentation. In the third reaction, decomposition of the target molecule occurs after its excitation. Both dissociative processes require closer vicinity of the reactants and occur efficiently at lower velocities [41], [42]. The last mechanism takes place when the target molecule has a permanent electric dipole moment. Then the ion−dipole interaction creates a transient complex even at relatively long projectile−target distances [45], [46], [48]. The present projectile is of molecular type (H_3^+); thus, either H_3^+ or H_3 can also be decomposed via dissociative excitation and dissociative recombination reactions [49], [50].

It is challenging enough to figure out explicitly in such kinds of experiments which mechanism appears and dominates. Although, some indications may be found through an in-depth examination of data. Since the apparatus used did not enable us to perform measurements of the absolute emission cross-sections, which are the most suitable for such an examination, we analyze the corresponding intensity ratios.

3.3.1. INTENSITY RATIOS

The charge transfer mechanism (CT) is here endoergic by about 0.3 eV (calculated using data from [51], [52]), and it is energetically the most favoured process. CT mechanism can be recognized using a simple method proposed in the [19] and [20] works. This routine is based on the observation that if the atomic charged projectile has its neutral counterpart in the ring structure, then the emission of this corresponding neutral item may come from the dissociation of neutralized

projectiles or fragmentation of the target molecules. In contrast, other fragments arise only due to the disintegration of the molecular ring. The intensity ratios calculated as quotients of this particular fragment intensity to the other products intensities are usually much higher than intensity ratios obtained for fragments stemming only from fragmentation, thus, suggesting the occurrence of CT reaction. In the H^+ collisions with THF [19], and furan [20], the $I_{H\beta}/I_{CH(A^2\Delta)}$ ratios were indeed several times higher than in the C^+/O^++THF [19], He^+/He^{++}+furan [46], and He^++pyridine [32] impact systems, respectively. Similarly, the $I_{C(2p3s\,^1P1)}/I_{CH(A^2\Delta)}$ ratios obtained in the C^+ collisions with THF were extremely large [19]. These observations can be explained in terms of the theoretical calculations of Erdmann *et al.* [45]. They calculated the energy curves and couplings of the C^{2+}+THF system and established strong delocalization of the electrons on the tetrahydrofuran ring toward the C^{2+} ion. As a result, single and double electron capture processes occurred.

In this regard, the intensity quotients of H(n=4) and CH($A^2\Delta$) fragments were checked. In Fig. 4, the $I_{H\beta}/I_{CH(A^2\Delta)}$ ratios for the H_3^++THF collisions are presented. At 80 km/s, the CH($A^2\Delta$) intensity is four times higher than H(n=4) intensity. This can be explained as follows. The reaction partners are very close at the lowest velocities, and mainly THF ring dissociates [41], [42]. Hydrogens most likely are detached from the ring. Although breakup of the neutralized projectile after charge transfer is less probable in this velocity range [41]-[44], it cannot be completely ruled out.

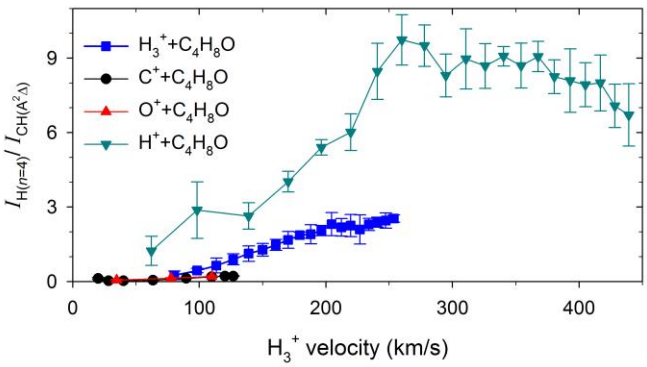

Fig. 4 – (Color online). The ratio of intensities of the H(n=4) and CH($A^2\Delta$) fragments in the collisions of H_3^+ with tetrahydrofuran. The ratios obtained from the THF fragmentation induced by proton [20] and the O^+ and C^+ [19] impact are shown for comparison.

Between 80-205 km/s, the intensity ratios increase linearly. The production of excited H atoms enlarges because both the neutralized ions and the target molecules undergo dissociation. Indeed, as the energy increases, the possibility of an electron jump from the target to the projectile rises [43]-[47]. When the cations keep getting faster, the interaction time is shortened. However, even at longer

distances, cations can feel the target molecules energy potential, enabling the charge transfer reaction to occur [47]. Indeed, recent *ab initio* calculations of the collisions of C^{q+} (q=2-4) carbon cations and protons (H^+) with deoxyribose (dR) [43], [44] showed that efficient electron charge transfer happens when the avoided crossings occur between the entrance channel (e.g. H^++dR) and the different electron transfer levels at the potential energy curves (for instance H+dR^+). Such avoided crossing was observed at a distance of R=2.5 Å, allowing charge capture at higher velocities. The avoided crossings around 2.0 Å have also been obtained in theoretical studies on collisions of C^{2+} ions with tetrahydrofuran [45] and He^+/He^{++} with furan [46], thus confirming the above scenario.

Above 205 km/s, the $I_{H\beta}/I_{CH(A^2\Delta)}$ ratios become stabilized. It seems that all competing reactions reach a specific state of equilibrium, and constant production of species is established.

Notably, intensity ratios obtained in the collisions of H^+ with THF generally show a similar shape, but they have much higher values. The trend consistency is understandable considering that in the collisions with protons, charge transfer from THF to H^+ was the dominant mechanism. On the contrary, the ratios obtained in collisions with O^+ and C^+ cations have negligibly small values, which is also apparent because, in these collisions, both the excited H and CH could arise only from the decomposition of the tetrahydrofuran ring.

3.3.2. BALMER DECREMENTS

The identification of the charge transfer process amongst the different collisional mechanisms in collisions where hydrogen atoms are incorporated into projectiles may also be made based on the analysis of the Balmer decrements defined as intensity ratios of Balmer series lines [20]. In quantum mechanics, these intensities are proportional to the principal quantum number n, according to the $I \sim n^{-3}$ relationship [53].

Therefore, the intensities of the Balmer lines were drawn in the log-log plot as a function of the principal quantum number n of the excited H(n) atoms, as shown in Fig. 5. Then, experimental points were approximated by an n^K exponential function, where K is a constant, using a weighted regression method with the weights proportional to the experimental errors. The K values were determined from the corresponding slopes of regression lines (solid blue lines in Fig. 5). The resulting K factors were plotted in function of projectiles velocity, as presented in Fig. 6. As can be seen, the K factors decrease almost exponentially. From –4 at 80 km/s, they quickly decrease to –6 (at 127 km/s). Between 128-254 km/s, they are approximately constant, reaching the lowest value of –6.9.

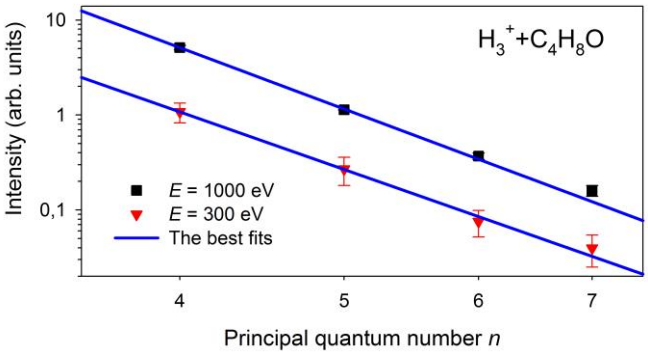

Fig. 5 – (Color online). Examples of the emission intensity of the lines of the Balmer series as a function of the principal quantum number *n*. The solid lines show the best fits to the points.

The present *K* factors can be compared with those obtained from the THF fragmentation induced by proton [20] and the O^+ and C^+ [19] impact (also shown in Fig. 6). The *K* factors obtained for protons follow a similar trend as the curve obtained in H_3^+ collisions but having a few percent lower values. Below 40 km/s velocities of C^+ cations, these factors were −3.0, and they decrease to –4.4 with the increase of the C^+ velocities. In contrast, the *K* values obtained in the O^+ impact are on average equal to –3.3.

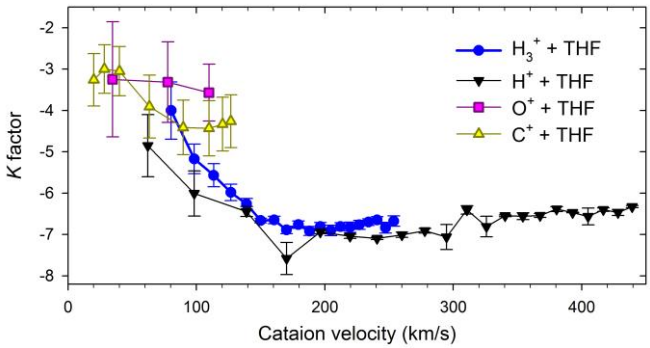

Fig. 6 – (Color online). The *K* factors as a function of projectiles velocity. The depopulation factors obtained from the fragmentation of tetrahydrofuran molecules into the H(*n*) atoms induced by proton [20] and the O^+ and C^+ [19] impact are shown for comparison.

Such low *K* values obtained in the present work indicate a rapid decrease in H(*n*) intensities with increasing principal quantum number *n*. Thus, the *K* factor defines the depopulation of higher excited states of hydrogen. Any deviation from the expected value may point to a specific collisional mechanism, as shown in [20]. If it is close to the theoretical value, hydrogen atoms are formed from the fragmentation of a target molecule due to dissociative processes. Such a situation is observed here at the velocity of 80 km/s. It was also detected for C^+ and O^+

collisions and in electron- [34] and photon-induced [16], [36] dissociation of heterocyclic molecules. If K is much lower than (–3), H(n) intensities decrease more quickly than in dissociation processes because other processes are responsible for forming the excited hydrogen atoms. For energetic reasons, the most probable process is electron transfer. The electron capture process indeed occurred and governed the collisions of protons with tetrahydrofuran [19], [20], and furan [20]. Taking into account the similarity of curves above 140 km/s for both H^+ and H_3^+ collisions, we conclude that the charge transfer process starts prevailing the H_3^+ interaction with THF at these velocities and the H(n) arise primarily due to electron transfer from THF to H_3^+ followed by dissociation of neutralized projectiles (H_3). Notably, the stabilization of $I_{H\beta}/I_{CH(A^2\Delta)}$ ratios (see Fig. 4) suggests complete dominance of this reaction at higher cation velocities.

4. SUMMARY

The collision-induced emission and the spectral signatures of collisional mechanisms occurring in the $H_3^+ + C_4H_8O$ impact system have been identified and compared with the results of the previous measurements. When light hadron collides polyatomic molecule, it does not cause substantial damage to it. Indeed, the luminescence spectra display a reduced set of excited atomic and diatomic products, similarly to collisions with protons. However, in contrast to H^+ impact, the H_3^+ irradiation enhances tetrahydrofuran ring fragmentation and leads to the more pronounced creation of CH radicals. The analysis of the $I_{H\beta}/I_{CH(A^2\Delta)}$ ratios and Balmer decrements suggest that charge transfer reactions dominate present collisions. Therefore, higher production of the excited hydrogen atoms H(n) most likely comes from projectiles dissociation. These findings agree with the ion-impact studies of Schlathölter and co-workers, who showed that the electron transfer mechanism releases most of the energy on the cation [41].

Acknowledgements. This article is based upon work from COST Action CA18212 – Molecular Dynamics in the GAS phase (MD-GAS), supported by COST (European Cooperation in Science and Technology). The experiments were carried out at the University of Gdansk using a spectrometer for the collision-induced emission spectroscopy. Therefore author thank prof. A. Kowalski (Univ. of Gdansk) and B. Pranszke (Gdynia Maritime Univ.) for enabling present measurements.

REFERENCES

1. Y. Furukawa, et al., Proc. Natl. Acad. Sci. U.S.A. **116**, 24440–24445 (2016).
2. R. Brédy, et al., J. Chem. Phys. **130**, 114305 (2009).
3. U. Amaldi, G. Kraft, Rep. Prog. Phys. **68**, 1861 (2005).
4. M. A. Huels, et al., J. Am. Chem. Soc. **125**, 4467 (2003).

5. I. Utke, et al., J. Vac. Sci. Technol. B **26**, 1197 (2008).
6. J.E.M. McGeoch, J. Microsc. **227,** 172-184 (2007).
7. L. P. Guler, et al., J. Phys. Chem. A **106**, 6754−6764 (2002).
8. C. J. Colyer, et al., J. Chem. Phys. **133**, 124302 (2010).
9. H. Müller, *Tetrahydrofuran* Ullmann's Encyclopedia of Industrial Chemistry. Weinheim: Wiley-VCH. doi:10.1002/14356007.a26_221.
10. S.-H. Lee, Phys. Chem. Chem. Phys. **12**, 2655-2663 (2010).
11. P. M. Mayer, et al., J. Phys. Chem. A **113**, 10923–10932 (2009).
12. A.A. Scala, et al., J. Chem. Phys. **108**, 7933 (1998).
13. A.A. Scala, W.J. Rourke, J. Photochem. **37**, 281-292 (1987).
14. A. Lifshitz, et al., J. Phys. Chem. **90**, 3422-3429 (1986).
15. J. Kramer, J. Phys. Chem. **86**, 26-35 (1982).
16. T. J. Wasowicz, et al., Phys. Rev. A **83**, 033411 (2011).
17. M. Dampc, et al., J. Phys. B: At. Mol. Opt. Phys. **44**, 055206 (2011).
18. D. Almeida, et al., J. Phys. Chem. A **118**, 690-696 (2014).
19. T.J. Wasowicz, B. Pranszke, J. Phys. Chem. A **119** (4) 581 (2015).
20. T.J. Wasowicz, B. Pranszke, Eur. Phys. J. D **70** (8) 175 (2016).
21. J. Pelley, ACS Cent. Sci. **5**, 741−744 (2019).
22. P. Drossart, et al., Nature. **340**, 539 (1989).
23. A. Yogo, et al., Appl. Phys. Lett. **94**, 181502 (2009).
24. H. Tsujii, et al., New J. Phys. **10,** 075009 (2008).
25. R. R. Allison, et al., Future Oncology **9**, 493-504 (2013).
26. F. Tommasino, et al., Int. J. Part. Ther. **2**, 428–438 (2016).
27. M. Durante, H. Paganetti, Rep. Prog. Phys. **79,** 096702 (2016).
28. A. Ehbrecht, et al., Chem. Phys. Lett. **284**, 205 (1998).
29. R. Drozdowski, A. Kowalski, Eur. Phys. J. D **72**, 220 (2018).
30. CSID:7737, http://www.chemspider.com/Chemical-Structure.7737.html (accessed 11:41, May 10, 2021)
31. T.J. Wasowicz, B. Pranszke, J. Phys. Chem. A **120**, 964 (2016).
32. T. J. Wasowicz, Res. Phys. **18**, 103244 (2020).
33. T. J. Wasowicz, J. Phys.: Conf. Series **635**, 032114 (2015).
34. I. Linert, et al., Chem. Phys. Lett. **498**, 27−31 (2010).
35. T. J. Wasowicz, et al., Photon. Lett. Pol. **3,** 110 (2011).
36. T. J. Wasowicz, et al., J. Phys. B: At. Mol. Opt. Phys. **45**, 205103 (2012).
37. M. Zubek, et al., J. Chem. Phys. **141,** 064301 (2014).
38. T. J. Wasowicz, et al., J. Phys. B: At. Mol. Opt. Phys. **47**, 055103 (2014).
39. T. J. Wasowicz, et al., J. Phys. B: At. Mol. Opt. Phys. **50,** 015101 (2017).
40. B. Pranszke, Chem. Phys. Lett. **484**, 24–27 (2009).
41. T. Schlathölter, et al., Phys. Scr. **73**, C113−C117 (2006).
42. S. Maclot, et al., ChemPhysChem **12**, 930−936 (2011).
43. M. C. Bacchus-Montabonel, J. Phys. Chem. A **118**, 6326−6332 (2014).
44. M. C. Bacchus-Montabonel, J. Phys. Chem. A **117**, 14169−1417 (2013).
45. E. Erdmann, et al., Phys. Chem. Chem. Phys. **19**, 19722-19732 (2017).
46. T.J. Wasowicz, et al., Int. J. Mol. Sci. **20**, 6022 (2019).
47. M. Akbulut, et al., Surf. Sci. Rep. **28**, 177-245 (1997).
48. R. D. Bowen, Acc. Chem. Res. **24**, 364−371 (1991).
49. S. Datz, et al., Phys. Rev. Lett**. 74**, 896 (1995).
50. M. J. Jensen, et al., Phys. Rev. A 63, 052701 (2001).
51. H. Helm, et al., Coupling of Bound States to Continuum States in Neutral Triatomic Hydrogen, in S. L. Guberman Edt., *Dissociative Recombination of Molecules with Electrons*, Springer Science+Business Media New York, 275-287, 2003.

52. P.J. Linstrom and W.G. Mallard, Eds., *NIST Chemistry WebBook*, NIST Standard Reference Database Number 69, National Institute of Standards and Technology, Gaithersburg MD, 20899, https://doi.org/10.18434/T4D303, (retrieved May 3, 2021).
53. H.E. Bethe, E.E. Salpeter, *Quantum Mechanics of One-and Two-Electron Atoms*. New York: Plenum Publishing Corporation (1977).